Confinement Effects In Supported *vs.* Isolated Quantum Structures: A Study of Si(001) Films

Chin-Yu Yeh, S. B. Zhang, S. Froyen and Alex Zunger
National Renewable Energy Laboratory, Golden, Colorado 80401
(Received 30 July 1993)

A conventional quantum well is a supported quantum structure whereas a free-standing film is an isolated quantum structure. The application of the effective mass particle-in-a-well approach (EMA) to quantum wells leads to the well-known quantization rule whereby the lowest, $j = 0$ quantum state is forbidden. The EMA identifies these forbidden states with the bottom of the potential wells at the band energy minima and maxima for each band n. Direct pseudopotential band structure calculations for free standing silicon films are compared here with such EMA solutions. While near the band energy *minima* the EMA wavefunctions agree with the results of the direct approach, they disagree completely near the band energy *maxima*. The standard EMA forbidden states Γ_{1v}, $\Gamma_{25'v}$, $\Gamma_{25'v}$, $\Gamma_{25'v}$, and Δ_{min} for n=1,2,3,4, and 5, respectively, are all *potential well minimum states*, whereas the forbidden states found in the direct calculation, Γ_{1v}, X_{1v}, X_{4v}, X_{4v}, Δ_{min} and X_{1c} for bands n=1,2,3,4,5 and 6, respectively, are all *band minimum energy states*. At the valence band maximum $\Gamma_{25'v}$, direct calculations reveal a novel quantum state of constant envelope functions, *whose energy does not vary with film's size*. Such a "zero confinement state" is absent in the EMA quantum well problem.

Keywords: Quantum Structure, Quantum Confinement, Si Film, Effective Mass

I. INTRODUCTION

Novel optical and electrical properties can be engineered through the control of size and dimensionality (D) of quantum structures in 0D (boxes), 1D (wires) and 2D (wells and films). Such structures can be either "supported" or "isolated". *Supported* quantum structures are coupled to another material with a similar underlying bulk electronic structure, *e.g.*, a GaAs well surrounded by an AlGaAs barrier. Such supported structures are treated successfully by the effective mass approximation (EMA) for a particle in an external potential well [1,2]. One can also consider *isolated* quantum structures such as a free-standing film: these are embedded in a medium lacking any quantum structure (*i.e.* vacuum). There is an important difference between a supported structure (*e.g.*, a 1D quantum well) and an isolated structure (*e.g.*, a 1D quantum film) which, as shown below, invalidates the EMA prescription for the latter case. This is illustrated in Fig. 1: A supported quantum well (Fig. 1a) is characterized by a sequence of *band (n, k_z)-dependent* potential wells with hights given by the appropriate band offset (typically $\sim$ 1eV in semiconductors). These wells can be concave (as is the case for the valence band minimum, VB_{min}, or the conduction band minimum, CB_{min} in Fig. 1a) or convex (*e.g.*, the valence band maximum, VB_{max} in Fig. 1a). The mini bands associated with a particular well are separated from those of other wells by energy continua (*i.e.*, extended scattering states) and by band gaps (*i.e.*, forbidden regions). These are depicted in Fig. 1a by the shaded areas. In the EMA these "electronic isolations" act to effectively cut-off much of the coupling between wells belonging to different (n, k_z) bands of the same material. Thus, in many cases one needs to consider quantization in one (n, k_z) well at a time. Consequently, the numbering of the EMA quantized levels starts with the quantum number $j_{\rm EMA}$=1 in *each* well, and the null solution $j_{\rm EMA}$=0 (corresponding to the minimum of the well) does not represent a probability wave and is thus disallowed. In the following, we will term the missing $j_{\rm EMA}$ in the quantum spectrum as a "forbidden state".

In contrast to a supported quantum well, in an isolated quantum film (Fig. 1b) numerous bands are confined by a *single*, concave well extending from the valence band *minimum*, all the way to the vacuum level ($\sim$ 20 eV in most covalent semiconductors). While the $j_{\rm EMA}$=0 state at the VB_{min} is still forbidden, just like

0749–6036/93/060141 + 08 $08.00/0

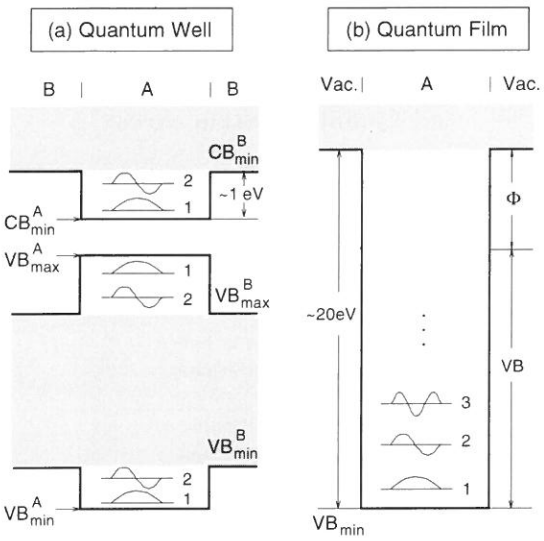

FIG. 1. Schematic depiction of quantum confinement in (a) a quantum well and (b) a quantum film. A and B denote well and barrier materials, respectively, whereas Vac. denotes vacuum. Φ is the work function. The shaded areas denote the region of energy continua. Energy levels and wavefunctions, indexed by quantum numbers $j_{\rm EMA}$, are shown schematically. Note that the convex wells are hole wells for which the quantum number $j_{\rm EMA}$ decends with the band energy.

in the supported quantum well case, the other ($n>1$) forbidden $j_{\rm EMA}$=0 states can be different. For example, since there is no distinct potential well at the film's VB$_{max}$, the corresponding $j_{\rm EMA}$=0 state (which is forbidden in a quantum well) could be allowed in a quantum film. We will see below that, in fact, unlike the quantum well case, *the forbidden states in a film correspond to the lowest energy states in each bulk band.*

The purpose of this paper is to explore the consequences of the qualitative difference between a (supported) 1D quantum well and an (isolated) 1D quantum film and points out the limitations of the effective mass model. We will compare the wavefunctions of a free standing Si film as obtained by the EMA and by an "exact" direct diagonalization of a realistic approximation to the film's Hamiltonian. We find that the effective mass description, which is appropriate for quantum wells, does not apply to quantum films. In particular, the film forbidden states obtained in the "exact" approach differ from those predicted by the EMA, as evidenced by the wavefunctions. A simple alternative (the "truncated crystal approach") to the EMA, which captures most of the features of the "exact" approach will then be offered.

II. THEORETICAL APPROACHES TO QUANTUM FILM WAVEFUNCTIONS

A. The Effective Mass Approximation

The electronic states of a quantum well can be rigorously described by considering the the well (W) material + the barrier (B) material as a (combined) solid in its own right. In this description both B and W are characterized by periodic potentials in their interiors and a potential step at the interface between them. The problem is then addressed by solving the band structure of B+W. The effective mass method approximates this problem by considering instead a particle in an *external* potential. The latter is taken to be *constant* inside B and W, with a physical band offset at the interface (Notice that the need for a slow varying potential with respect to the unit cell size has been dropped here, making the application of the EMA to large offset systems questionable.) In doing so, one replaces the bulk band structure $\epsilon^{bulk}_{n,\mathbf{k}}$ by a (band index n dependent) pure kinetic energy form

$$\epsilon^{EMA}_{n,\mathbf{k}} = \epsilon_{n,\mathbf{k_0}} + \frac{\hbar^2(\mathbf{k}-\mathbf{k_0})^2}{2m^*_{n,\mathbf{k_0}}} \quad , \tag{1}$$

where $\epsilon_{n,\mathbf{k_0}}$ and $m^*_{n,\mathbf{k_0}}$ are the band edge energy and effective mass at $\mathbf{k_0}$. One further replaces the bulk eigenstates $\psi^{bulk}_{n,\mathbf{k}}(\mathbf{r})$ by $\psi^{EMA}_{n,\mathbf{k}}(\mathbf{r})$ which is a product of an envelope function $f_{\mathbf{k}-\mathbf{k_0}}(\mathbf{r})$ and a fixed $\mathbf{k_0}$ Bloch periodic piece $u_{n,\mathbf{k_0}}(\mathbf{r})$. This transforms the boundary problem of a finite solid into a particle-in-a-box problem for $f_{\mathbf{k}-\mathbf{k_0}}(\mathbf{r})$. For concreteness, consider the zone center states ($\bar{\Gamma}$: $k_x = k_y = k_{x0} = k_{y0} = 0$) of a (001)$\equiv z$-oriented Si quantum film of thickness $L = Na/4$, where N is the number of monolayers and a is the bulk cubic lattice constant. The requirement that the wavefunction $\psi^{EMA}_{n,\bar{\Gamma}}(\mathbf{r})$ will vanish at the boundaries leads to an envelope function represented by a *sine*-like standing wave created by a destructive interference between two running plane waves of opposite directions, *i.e.*,

$$\psi^{EMA}_{n,\bar{\Gamma}}(\mathbf{r}) = u_{n,k_{z0}}(\mathbf{r}) sin(k_z - k_{z0})z \quad . \tag{2}$$

The ensuing quantization conditions are

$$k_z - k_{z0} = \frac{\pi}{L} j_{\rm EMA} = \frac{2\pi}{a}\,\frac{2j_{\rm EMA}}{N}; \qquad |j_{\rm EMA}| = 1,2,3,\ldots \quad , \tag{3a}$$

where

$$k_z = \frac{2\pi}{a}\,\frac{2j}{N}; \qquad k_{z0} = \frac{2\pi}{a}\,\frac{2j_0}{N} \quad . \tag{3b}$$

The quantum numbers, j, j_0 and $j_{\rm EMA}$ satisfy therefore the relation

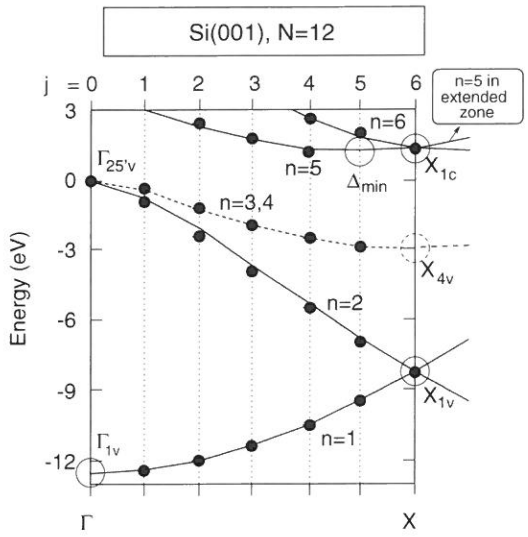

FIG. 2. Silicon bulk band structure. The solid and dashed lines of index n denote single and twofold degenerate bands, respectively. The figure also shows the mapping of a 12 layer film states of the direct approach (solid dots) to those given by $\epsilon^{film}_{f,\bar{\Gamma}} = \epsilon^{bulk}_{n,k^*_z}$. The latter are given by intersections of the vertical dotted lines at j with the bulk dispersion. Forbidden j's are shown as large open circles.

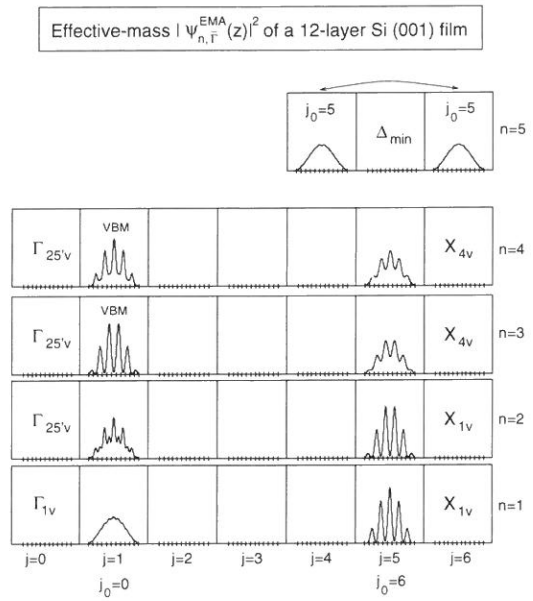

FIG. 3. x-y planar averaged wavefunctions $|\psi^{EMA}_{n,\bar{\Gamma}}(z)|^2$ of a 12-layer Si (001) film obtained by the EMA. j indexes k^*-vector and n is the band index. The value of j_0 corresponding to the band extrema (used by the EMA) are indicated. Symmetry labels, $\Gamma_{25'v}$, Γ_{1v}, X_{1v}, X_{4v}, and Δ_{min}, denote EMA forbidden states. The ticks in the horizontal axis denote the atomic planes. The arrow in the upper panel denotes that the two states are identical.

$$j = j_{\rm EMA} + j_0 \quad . \tag{3c}$$

Note that the state at $k_z = k_{z0}$ (corresponding to $j_{\rm EMA} = 0$ and $j = j_0$) is forbidden. The EMA identifies this forbidden state with the *minimum of the appropriate potential well* (and is hence band index n dependent). For example, in bulk Si (whose band structure is shown in Fig. 2), the Γ_{1v} state of band n=1 constitutes the bottom of the VB_{min} potential well (Fig. 1a), so $k_{z0} = \Gamma_{1v}$ in Eq. (3) is forbidden. Likewise, the $\Gamma_{25'v}$ states of bands n=2,3,4 are taken as the minima of the VB_{max} (hole) potential wells, so $k_{z0} = \Gamma_{25'v}$ is forbidden too. In the n=5 conduction band the minimum is at Δ_{min}, so $k_{z0} = \Delta_{min}$ is forbidden. Thus, the EMA approach excludes from the spectrum of Si quantum wells the states Γ_{1v}, $\Gamma_{25'v}$, and Δ_{min} which are *potential well minimum states*. Note that in general, potential well minimum states can differ from *band minimum states*: Fig. 2 shows that the latters (denoted as large open circles) are Γ_{1v}, X_{1v}, X_{4v}, X_{4v}, for bands n=1,2,3, and 4, respectively.

We have calculated the EMA wavefunctions for a 12 layer (001) Si quantum film. Figure 3 shows the xy-averaged wavefunction amplitude $|\psi^{\rm EMA}_{n,\bar{\Gamma}}(z)|^2$. The well-minimum Bloch functions $u_{n,k_{z0}}(\mathbf{r})$ appearing in Eq. (2) were calculated from the bulk pseudopotential band structure (see below). Because the EMA is valid only in the region $k - k_0 \ll \frac{2\pi}{a}$, we show in Fig. 3 the EMA wavefunctions just for $j_{\rm EMA}$=1. We have sorted in Fig. 3 the calculated wavefunctions according to the quantum number j [Eq. (3)] and the bulk band index n. n and j appear along the x and y axis of Fig. 3, respectively. The band-edge points k_{z0} (or, alternatively, the value of j_0) were selected as follows. For n=5, we take $k_{z0} \sim \Delta_{min}$, so $j_0 = 5$. For n=1,2,3, and 4, we use $j_0 = 0$. Besides these standard EMA choices of j_0 in Fig. 3, we also use for comparison $j_0 = 6$ for zone boundary states for n = 1,2,3,4. The EMA-forbidden states are denoted in Fig. 3 by their symmetry labels, *i.e.* Γ_{1v}, $\Gamma_{25'v}$, and Δ_{min}, etc.

B. The Direct Diagonalization Approach

To assess the validity of the EMA results for a film (Fig. 3), we have calculated independently the film's wavefunctions from a direct diagonalization approach which is free of effective mass approximations. We solve

$$[-\frac{1}{2}\nabla^2 + V^{film}(\mathbf{r})]\psi_f^{film}(\mathbf{r}) = \epsilon_f^{film}\psi_f^{film}(\mathbf{r}) \quad , \qquad (4)$$

where $V^{film}(\mathbf{r})$ is the potential of the film constructed here from a superposition of atomic pseudopotentials. Equation (4) was solved by imposing periodic boundary conditions on the N-layer film straddled by N_{vacuum} layers of vacuum. This transforms the film problem into a Bloch-periodic band structure problem, solved by expanding ψ_f^{film} in plane waves. We increase N_{vacuum} until the results are independent of it to within 0.02 eV. Since the EMA does not consider surface effects, we try to mimic this situation also in the direct diagonalization approach of Eq. (4). To this end we have used a non-self-consistent empirical pseudopotential description here rather than a self-consistent one, because the latter propagates the unwanted surface effects deeper into the interior of the film. The atomic Si pseudopotentials used to construct V^{film}(r) of Eq. (4) were fitted both to the bulk band structure and to the Si work function ($\sim$ 4.9 eV) [3,4]. This was done to assure that the confinement potential of Fig. 1b is realistic. The Si bulk band structure is shown in Fig. 2. We use the same pseudopotential approach to calculate the Bloch-periodic functions $u_{n,k_{z0}}$(r) of Eq. (2) and Fig. 3. The "direct diagonalization" approach of Eq. (4) includes in a natural way the periodic potential of the film material as well as the "potential well" outside it. No implication is made that the solutions are valid only near band edges or that the dispersion relations are parabolic. The only approximation involved is the use of an empirical pseudopotential, which, however, is fit to a realistic form. Hence, this "exact" approach will be used as a benchmark against which the EMA results will be compared.

Figure 4 depicts the directly calculated film wavefunctions $|\psi_{f,\Gamma}^{film}(z)|^2$ for a 12 layer Si(001) film up to n = 6. The near-Γ states for band n=5,6 are omitted since they are too close to the vacuum level and are thus not completely confined.

It is useful to sort out the directly calculated film wavefunctions according to bulk bands, so a comparison with the EMA results of Fig. 3 can be made. While the EMA states are constructed from an interference of *plane waves* of opposite propagation directions, an appropriate basis for the *directly* calculated film wavefunctions is given by an interference of *Bloch waves*, *i.e.*

$$\chi_{n,k_z}(\mathbf{r}) = \begin{cases} \psi_{n,k_z}^{bulk}(\mathbf{r}) - \psi_{n,-k_z}^{bulk}(\mathbf{r}) & \text{if } 0 \le z \le L \quad ; \\ 0 & \text{if } z < 0 \text{ or } z > L \quad . \end{cases} \qquad (5)$$

Since $\psi_{n,-k_z}^{bulk}(\mathbf{r}) = [\psi_{n,k_z}^{bulk}(\mathbf{r})]^*$, Eq. (5) can be rewritten for $0 < z < L$ as

$$\chi_{n,k_z}(\mathbf{r}) = \sqrt{2} \quad [u_{n,k_z}^R(\mathbf{r})sin(k_z z) + u_{n,k_z}^I(\mathbf{r})cos(k_z z)] \quad , \qquad (6)$$

where $u_{n,k_z}^R(\mathbf{r})$ and $u_{n,k_z}^I(\mathbf{r})$ are the real and imaginary parts of the bulk $u_{n,k_z}(\mathbf{r})$, and k_z is quantized as

$$k_z^* = \frac{\pi}{L}j = \frac{2\pi}{a}\frac{2j}{N}; \qquad j = 0, 1, 2, ..., N/2 \quad . \qquad (7)$$

Equation (7) differs from Eq. (3a) in that no forbidden state j_0 is assigned *a priori*. Equations (6) and (7) define a set of orthornormal and complete "truncated crystal basis functions" [3,4]. The zone center film (f) state, $\psi_{f,\Gamma}^{film}(\mathbf{r})$, can thus be expanded [3,4] as

$$\psi_{f,\Gamma}^{film}(\mathbf{r}) = \sum_n \sum_{k_z^*} a_{n,f}(k_z^*)\chi_{n,k_z^*}(\mathbf{r}) \quad . \qquad (8)$$

The expansion coefficients are calculated from

$$a_{n,f}(k_z^*) = < \psi_{f,\Gamma}^{film} | \chi_{n,k_z^*} > \quad , \qquad (9)$$

using Eq. (6) for χ_{n,k_z^*} and the solutions $\psi_{f,\Gamma}^{film}$ from Eq. (4). The projections $|a_{n,f}(k_z^*)|^2$ can then be used to (i) find which k_z^* values are forbidden in the film (*i.e.*, states with null projection), (ii) identify the parentage of the directly calculated film states in terms of bulk bands, and (iii) identify surface states.

The calculated projections (shown in % as inserts to Fig. 4) reveal that: (i) Each *valence band* film state evolves essentially from a single bulk state of band n at a special k_z^* of Eq. (7). In this case, the boundary conditions at $z = 0$ and $z = L$ are satisfied, in the first part of Eq. (6), by the sine envelope function and, in the second part of Eq. (6), by the nodal planes of $u_{n,k_z}^I(\mathbf{r})$. (ii) Conduction band film states are found to evolve from two bulk states. This is because for $n = 5$, $k_0 = \Delta_{min}$ is neither a zone center nor a zone boundary point. In order to satisfy the boundary conditions at (0,L) the destructive interference takes place between states at k_z and $2\Delta_{min} - k_z$ in the extended zone (Fig. 2). This translates into two k-points in the first zone: (n,k_{z1}^*) and (m,k_{z2}^*). For example, the (n,k_{z1}^*)=(n=5, j=4) state couples with the (m,k_{z2}^*)=(n=5, j=6) state, and the (n,k_{z1}^*)=(n=5, j=3) state couples with the (m,k_{z2}^*)=(n=6, j=5) state, etc. These are represented by the arrows in the conduction bands of Fig. 4. Hence, in this case

$$\psi_{f,\Gamma}^{film}(\mathbf{r}) \approx a_{n,f}(k_{z1}^*)\chi_{n,k_{z1}^*}(\mathbf{r}) + a_{m,f}(k_{z2}^*)\chi_{m,k_{z2}^*}(\mathbf{r}) \quad . \qquad (10)$$

The inserted numbers for conduction band states in Fig. 4 give the appropriate *sum* of the two state projections. The fact that a film state couples only to one or two truncated crystal basis functions suggests that the basis set given by Eq. (6) is an optimal choice.

Figure 4 sorts out the directly calculated film wavefunctions according to the quantum number j of Eq. (7) as well as the band index n for which there is a max-

imum projection. This sorting establishes a correspondence with the EMA wavefunctions of Fig. 3. Note that while the direct approach provides *all* film wavefunctions (Fig. 4), in the EMA (Fig. 3) only near band edge wavefunctions (small j or large j) are meaningful. Like in Fig. 3, forbidden states are denoted in Fig. 4 by their symmetry labels, *i.e.* Γ_{1v}, X_{1v}, X_{4v}, etc. States evolving into surface states are marked as SS.

It is immediately evident that *the EMA identifies incorrectly some of the forbidden states*: the EMA forbidden states Γ_{1v}, $\Gamma_{25'v}$, $\Gamma_{25'v}$, $\Gamma_{25'v}$, and Δ_{min} for n=1,2,3,4, and 5, respectively, are all *potential well minimum states*, whereas the forbidden states found in the direct calculation, Γ_{1v}, X_{1v}, X_{4v}, X_{4v}, Δ_{min} and X_{1c} for n=1,2,3,4,5 and 6, respectively, are all *band minimum energy states* (see Fig. 2). This is discussed next.

III. WAVEFUNCTION PATTERNS

Comparing the wavefunction patterns of Fig. 3 with those of Fig. 4, we see that:

(i) The EMA provides a good approximation to the states near the true energy band minima, Γ_{1v} and X_{4v}.

(ii) The EMA works less satisfactorily for states near Δ_{min} (in Fig. 3a), because an effective mass approximation gives only the sine modulation and cannot tell the differences between states on the left-hand side and on the right-hand side of Δ_{min}. In the direct diagonalization approach, the states on these two sides are different: one is sine-type and the other is cosine-type (see below).

(iii) The EMA is incorrect for states near $\Gamma_{25'v}$ and X_{1v}. For n =3,4, the j=1 states should be cosine-like and sine-like [Eq. (6)], respectively, as shown in Fig. 4. Also at n =3, the EMA rules out the j=0 state which exists in the direct approach (Fig. 4) with a constant envelope function. The patterns do not agree for the states near X_{1v}, and in addition a j=6 and n=1 state does not exist in Fig. 3c but exists in Fig. 4.

We expect that the failure of the EMA near $\Gamma_{25'v}$ (in Fig. 3) cannot be fixed by multi-band coupling schemes such as the Luttinger model [5] which still relys on the assumption of hole confinement. Since the truncated crystal basis set of Eq. (6) has a near 100% projection on the films states (Fig. 4), we can inspect its form to see why even multi-band effective mass models are still insufficient: Equation (6) shows that realistic film's wavefunctions need not to have k_0 dependence but instead they allow cosine-type modulation. The cosine component satisfies the boundary conditions by the nodal structure of the Bloch-periodic function $u_{n,k_z^*}(\mathbf{r})$, not by the envelope function as is the case in the EMA. For example, materials whose atoms exhibit but s valence orbitals (*e.g.*, hydrogen) have nodeless $u_{n,k}(\mathbf{r})$, so the boundary conditions in films made of such atoms must

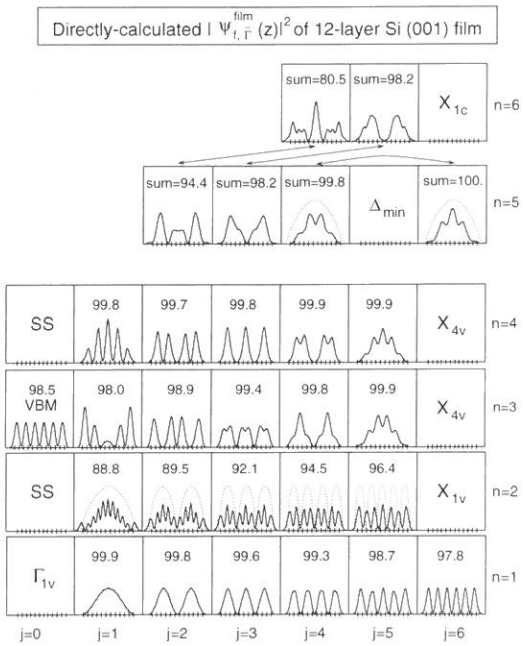

FIG. 4. x-y planar averaged wavefunctions $|\psi^{film}_{f,\bar{\Gamma}}(z)|^2$ of a 12-layer Si (001) film obtained by the direct approach (solid lines). Schematic drawing of the global peaks at n=2 and 5 are represented by the dotted lines. j indexes the k_z^*-vector and n is the band index. "SS" denotes film surface states. Symmetry labels, Γ_{1v}, X_{1v}, X_{4v}, X_{4v}, X_{1c} and Δ_{min}, denote the forbidden states. The inserted numbers show the bulk projections in percent. Arrows in the upper panel denote the paired k_z^*'s in Eq. (10). "sum" means the sum of the projections of a film state to these paired bulk states.

be satisfied by the envelope functions (which hence must be sine-type). This is also the case for Si film states evolving from the s-like n=1 band. On the other hand, materials with valence bands derived from atomic p, d orbitals may have $u_{n,k_z^*}(\mathbf{r})$'s with nodal structures, so for some film states *the boundary conditions could be satisfied by the Bloch function rather than by the envelope function*. This feature is absent in either single-band or multi-band EMA and leads to the significant differences in film wavefunctions noted in Fig. 3 *vs.* Fig. 4.

Before comparing Fig. 3 and Fig. 4 in detail, two comments are pertinent: (a) In general, the nodal structure of $u_{n,k_z^*}(\mathbf{r})$ and that of the envelope function could create interference patterns. We thus expect complex wavefunction patterns both in the EMA, where u_{n,k_0} interferes with $\sin[(k_z - k_{z0})z]$, and in the general solution of Eq. (6) where u_{n,k^*} can interfere both with sine and cosine envelope functions. (b) The projection $|a_{nf}|^2$ reveals that the directly calculated Si film states

are either nearly-pure-sine or nearly-pure-cosine states: *e.g.* the film states evolving from band n=1,2,4 and 6 are sine-like, whereas the film states evolving from n=3 and 5 are cosine-like. With these general comments, we next discuss the wavefunction patterns of Fig. 4 in some detail:

(i) For n=1: the number of peaks (n_p) correlates with the quantization index j, *i.e.*, $n_p = j$. This is what we expected.

(ii) For $n = 2$: $\{\psi^{film}(\mathbf{r})\}$ show a complex pattern (Fig. 4) with both fine (solid lines) and global (dotted lines) peaks. In moving from $j = 1$ to $j = \frac{N}{2} = 6$, the number of global (G) peaks (n_G) increases from one to five, in line with the change of j. The number of fine (F) peaks n_F = N-j changes from 11 to 7 as j changes from 1 to 6. Using an extended zone scheme, these fine peaks can be viewed as an extension of the peaks in the $n = 1$ band.

(iii) For $n = 3$: (a) an EMA-forbidden $j_0 = 0$ state is present, with a constant envelope function (zero confinement state), and (b) the j=1 state has an envelope function maxima near the boundaries of the film, in contrast to the EMA solutions where the maxima are in the interior of the film.

(iv) For $n = 4$: as for $n = 2$, the wavefunction patterns can also be sorted as global and fine peaks. A simple relation between the peak numbers with j is obtained by assuming that the global peaks at small j's evolve into fine peaks at large j's, and vis versa. This is shown in Fig. 5 where the global peak sequence at small j's is labeled as $n_{Gs} = j$ and at large j's is labeled as $n_{Gl} = \frac{N}{2}$-j. This kind of sorting also works for the $n = 3$ band. In contrast to the $n = 4$ band where the two peak sequences are both sine-like, for $n = 3$ the Gs is, however, cosine-like while the Gl is sine-like (Fig. 5).

(v) For $n = 5$ and 6: while it is difficult to sort out all the fine peaks, the global peaks (dotted lines in Fig. 4) follow $n_G = |j - j_0| = |j - 5|$. States to the left of Δ_{min} in Fig. 4 are cosine-like; states to the right (n=5, j=6) and those in the $n = 6$ band, *i.e.* (n=6, j=5), (n=6, j=4) etc. are sine-like.

Here, we summarize the wavefunctions patterns given by the direct approach:

$$n = 1: \qquad n_p = j \quad , \tag{11a}$$

$$n = 2: \qquad \begin{cases} n_G = j & ; \\ n_F = N - j & , \end{cases} \tag{11b}$$

$$n = 3 \text{ and } 4: \qquad \begin{cases} n_{Gl} = j & ; \\ n_{Gs} = \frac{N}{2} - j & , \end{cases} \tag{11c}$$

$$n = 5 \ (\textit{including } n = 6): \qquad n_G = |j - j_0| \quad , \tag{11d}$$

where $N = 12$ and $j_0 = 5$ for the 12-layer Si(001) film.

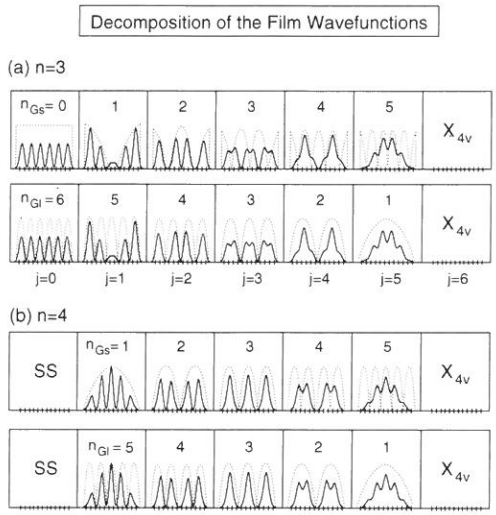

FIG. 5. Schematic drawing of the decomposition of the film wavefunction (solid lines) into small-j-global (G_s) and large-j-global (G_l) peaks (dotted lines) for n=3 and 4. The inserts are the number of the peaks n_{Gs} (n_{Gl}) of the envelope functions which increase as j increase (decrease). Note that for n=3, G_s consists of peaks centered at the boundaries. Two boundary (half) peaks are counted as one peak in the figure and Eq. (11).

IV. ENERGY LEVELS AND THEIR EVOLUTION WITH SIZE REDUCTION

The layout of Fig. 4 and the fact that a near 100% bulk projection value is achieved for most of the film states suggest that one can set up an energy map between film energy eigenvalues ϵ^{film} and the bulk band structure ϵ^{bulk} at the specified (n, k_z^*) points:

$$\epsilon^{film}_{f,\Gamma} \approx \epsilon^{bulk}_{n,k_z^*} \quad . \tag{12}$$

This is tested in Fig. 2, where the solid dots denote the directly calculated film eigenvalues $\epsilon^{film}_{f,\Gamma}$, and the dotted vertical lines give the quantized k_z^* values of Eq. (7). The intersections of the dotted lines with the bulk band structure give $\epsilon^{bulk}_{n,k_z^*}$. The amount by which these intersections miss the solid dots thus gives the error in Eq. (12). We see from Fig. 2 that Eq. (12) works very well. A comparison between the EMA energy levels and those of the direct calculations is given in Table I. In contrast to the wave functions, the EMA energy levels appear to agree reasonably well with those of the direct approach for N=12. However, as the film thickness reduces, the EMA results often get worse because the bulk energy despersion for larger $k \sim \frac{1}{L}$ is less parabolic. This is discussed further in Ref [3,4]. In what follows we use

TABLE I. Comparison of the energy levels (in eV) of states in the nth band and jth quantum number, (n,j). $\Delta\epsilon = \epsilon_{\text{Direct}} - \epsilon_{\text{EMA}}$.

	N=8				N=12		
(n,j)	EMA	Direct	$\Delta\epsilon$	(n,j)	EMA	Direct	$\Delta\epsilon$
(1,1)	-12.30	-12.23	0.07	(1,1)	-12.45	-12.42	0.03
(2,1)	-1.68	-1.79	-0.11	(2,1)	-0.75	-0.91	-0.16
(3,1)	-1.14	-0.77	0.37	(3,1)	-0.51	-0.42	0.09
(3,3)	-2.71	-2.70	0.01	(3,5)	-2.86	-2.86	0.00
(4,1)	-1.13	-0.77	0.36	(4,1)	-0.51	-0.41	0.10
(4,3)	-2.71	-2.70	0.01	(4,5)	-2.86	-2.86	0.00
(5,2)	1.56	1.65	0.11	(5,4)	1.38	1.35	-0.03
(5,4)	1.56	1.45	-0.11	(5,6)	1.38	1.23	-0.15

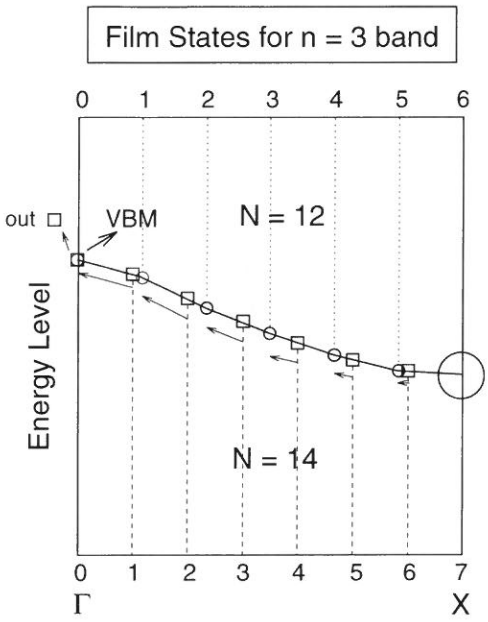

FIG. 6. Energy relation between 12 layers (small circle) and 14 layers (square) films. The large circle denotes the forbidden X_{1v} state. The solid line represents the bulk Si $n = 3$ band.

Eq. (12) to study the evolution of energy levels with size reduction.

Figure 6 shows the film states derived from the $n = 3$ band which includes the VBM state $n = 3$, $j = 0$ of Fig. 4. It shows the energy eigenvalues for two film thicknesses: $N = 12$ and 14 (dots and squares, respectively). The solid line denotes the bulk energy dispersion. The forbidden $\mathbf{k} = \mathbf{k_0}$ at the X point is denoted by a large open circle. Although we discuss here only the $n = 3$ band, the general conclusions apply to any other band. We see from Fig. 6 the following:

(i) The forbidden $\mathbf{k_0}$ state is fixed for any N at the *bottom* of the $n = 3$ band. It is a general observation that in free-standing films, states at the bulk band *minima* (not at the EMA potential well minima) are eliminated due to quantum confinement.

(ii) With the decrease of N from 14 to 12, each N = 14 (square) state evolves into a N = 12 (circle) state along the trajectory determined by the bulk band structure (the solid line). The motion (indicated in Fig. 6 by arrows) is away from the forbidden state at X towards Γ. In the EMA, this takes place along the trajectory of *parabolic* bands [Eq. (1)], leading to the familiar $\epsilon \propto \frac{1}{N^2}$ behavior. In a more realistic description, however, it occurs along the actual (possibly non-parabolic) bulk band.

(iii) The horizontal k-space separation between any two adjacent states [proportional to $\frac{1}{N}$, see Eq. (7)] increase as N decreases. Thus, the total number of states in the band ($= \frac{N}{2}$) decreases: it is 7 for $N = 14$ and 6 for $N = 12$. The net effect of (i)-(iii) is that a size reduction reduces the number of confined states in each band by expelling states from the *top of the band* (VBM in Fig. 6) to the gap region. In contrast, in the EMA approach it is assumed that states at the top of the potential wells (whether they are band energy minima or band energy maxima) are expelled to the energy continua (see Fig. 1a).

(iv) Despite the change in number of confined states, there is a $j = 0$ state for both $N = 14$ and 12, corresponding to the constant envelope function "zero confinement state" in Fig. 4. The energy of this state is pinned at the bulk VBM level and is independent of layer number N. Hence, for even layered free-standing Si(001) films there is no confinement-related energy shift at the VBM.

V. SUMMARY

We presented wavefunction patterns for Si(001) films using a direct Hamiltonian diagonalization approach. Due to the fundamental difference between the confining potentials between free standing quantum films and supported quantum wells, these wavefunction pattern have important difference from those of quantum wells. In particular, projecting these wavefunctions onto bulk states shows that: (i) states near the band energy *minima* resemble closely to those of the wells, described by an effective-mass particle-in-a-box approach while (ii) states near the band energy *maxima* are totally different, containing effectively cosine-type envelope functions in addition to the well known sine-type envelopes. Use of a combined sine/cosine "truncated crystal" basis allows us to describe the film states fully in terms of their parent bulk states. A simple relation between the shape,

the number of peaks of a film state and its quantum index (n, j) is found. The evolution of energy levels with film layer thickness is examined, revealing the importance of non parabolic energy dispersion and the lack of quantum confinement at the top of valence band.

Acknowledgement—This work was supported by the Office of Energy Research, Division of Materials Science, U. S. Department of Energy, under contract DE-AC02-83-CH10093.

REFERENCES

[1] G. Bastard, *Wave Mechanics Applied to Semiconductor Heterostructures*, (Les editions de physique, Les Ulis, 1988), p63.
[2] R. Dingle, W. Wiegmann and C. H. Henry, Phys. Rev. Lett. **33**, 827 (1974).
[3] S. B. Zhang and A. Zunger, Appl. Phys. Lett. **63** 1399 (1993).
[4] S. B. Zhang, C.-Y. Yeh, and A. Zunger, Phys. Rev. B**48**, 11204 (1993).
[5] J. M. Luttinger, Phys. Rev. **102**, 1030 (1956).